飞秒激光烧蚀单壁碳纳米管制备碳炔

陈文彬[1]，冯吉军[1*]，廖洋[2]，夏新成[1]，蒋巍[1]，任文波[1]，骆涛[3]，赵新洛[3**]

[1]上海理工大学光电信息与计算机工程学院上海市现代光学系统重点实验室，上海 200093；
[2]中国科学院上海光学精密机械研究所强场激光物理国家重点实验室，上海 201800；
[3]上海大学低维碳与器件物理研究所物理系，上海 200444

摘要 利用重复频率为 1 kHz 的钛蓝宝石飞秒激光烧蚀悬浮在甲醇中的单壁碳纳米管制备碳炔。利用表面增强拉曼光谱仪和紫外可见吸收光谱仪对样品溶液进行光谱表征，并用高效液相色谱仪对样品进行分离，确认有碳炔（C_nH_2，$n=6,8,10,12,14,16$）生成，其中的主要产物是 C_8H_2。对制备碳炔的最佳激光功率与最佳加工时间进行了研究，结果显示：当激光单脉冲能量为 0.52 mJ、加工时间为 1.5 h 时，可以获得最高的碳炔产率。对碳炔的合成机制进行了较深入的解释。激光功率密度存在饱和阈值，该饱和阈值与 C_2 自由基的碎裂程度有关，激光功率密度超过饱和阈值后会打破 C_2 自由的"反向"第四键，进而影响 C_2 自由基合成碳炔。因此，随着激光单脉冲能量增大，碳炔的产率呈现先增加后降低的现象。本研究可为碳炔的大规模制备提供重要参考。

关键词 激光技术；碳炔；飞秒激光烧蚀；激光功率密度饱和阈值；单壁碳纳米管

中图分类号 TN249　　　**文献标志码** A　　　**DOI:** 10.3788/CJL230610

1 引　言

碳的结构主要可分为一维结构（sp）、二维结构（sp^2）和三维结构（sp^3）。一维结构的典型代表是碳炔，二维结构的典型代表是石墨，三维结构的典型代表是金刚石。本次实验中制备是碳的一维结构——碳炔，其分子是为 $C_{2n}H_2$，是由碳碳单键和碳碳三键[1]交替连接组成的一维线性材料，而且也是"卡拜"的稳定分子形式[2-4]，其碳链可以趋于无限长[5]。碳炔具有优异的电学性能（例如导电和电子输运性能[6]）以及极高的硬度（硬度是金刚石的 40 倍[7]），在航空航天和纳米技术中都有潜在应用。将碳炔插入碳纳米管中可以形成稳定的长链碳炔[8-9]。碳炔是构建富勒烯的基础[10]，因此在下一代纳米器件中具有重要作用。目前，最长的一个碳炔由 44 个相邻的乙炔碳组成，它保持着碳碳单键和碳碳三键交替连接的框架结构[11]。碳炔的合成方法有多种，大致可分为电化学法（例如氧化偶联法和电弧法）和激光烧蚀法（例如气相激光烧蚀法和液相激光烧蚀法）。氧化偶联法很复杂并且容易引入杂质[12]。电弧法通常在水中通过电弧放电生成碳链[13-14]，但它不能控制碳链两端的基团。基团决定了碳炔的稳定性和电学性质，如果不能控制两端的基团就会产生很多副产物，碳炔优异的电学性能就无法展现。对于激光烧蚀法来说，气相激光烧蚀实验设备比较复杂，要求气密性高和温度稳定[15-16]；相比较而言，液相激光烧蚀法的成本相对较低并且便于更换多种靶材，因此已被广泛用于室温下制备碳纳米结构[17]。采用激光烧蚀法合成的碳炔具有自由基性质，因为聚合反应被认为是通过添加 C_2 自由基或 C_2H_2 基而发生的[18]。液相脉冲激光烧蚀的物理学研究表明，碳炔形成于激光烧蚀的等离子体羽流与溶剂之间的界面上，此处呈强烈的不平衡状态，可形成自由基。对于液相激光烧蚀来说，最常用的是纳秒激光或飞秒激光。相比较而言，纳秒激光的热效应较高，不利于室温下形成碳炔[19-20]，而飞秒激光具有热效应低和光子能量高的特点，有利于打破单壁碳纳米管的化学键，从而制备碳炔[21]。

有人研究了前驱体和有机溶液的比例与产率的关系[18]，还有人介绍了预热前体对碳炔产率的影响以及银溶胶对碳炔拉曼光谱的影响[22]。理想的长线性碳链是无限长的 sp-杂化碳链，通常将其称为"碳炔"。许多理论计算都是基于无限长的碳炔进行的，然而目前在实验室中只能得到有限长的碳炔[23]。若要合成非常长的碳炔，则需要将制备的碳炔溶液进一步加工，将碳炔插入末端开放的单壁碳纳米管中，然后进行高温高压处理，使短链碳炔融合生长成长链碳炔[24-25]。有人采用飞秒激光照射液体烷烃制备了碳炔，并依据碳炔的

形成机理提出了如下观点：主要反应序列是激光焦点处发生的带正电荷的碳物质的扩散[26]。目前尚未看到飞秒激光功率密度对碳炔最佳制备条件影响的相关报道。鉴于此，笔者利用重复频率为 1 kHz 的钛蓝宝石飞秒激光器烧蚀悬浮在甲醇中的单壁碳纳米管制备碳炔，并探索了制备碳炔的最佳激光功率与最佳加工时间。单脉冲能量为 0.52 mJ 时，碳炔的产率最高。对比不同加工时间下制备的碳炔发现飞秒激光的最佳烧蚀时间为 1.5 h，这为飞秒激光液相激光烧蚀制备碳炔提供了重要参考。此外，本文对碳炔的合成机理进行了深度解释，并提出了"激光功率密度饱和阈值"这一概念，其与 C_2 自由基的碎裂程度有关[27]。激光功率密度超过饱和阈值后会影响 C_2 自由基合成碳炔，因此，随着激光单脉冲能量增加，碳炔的产率呈现先增大后降低的现象。在激光脉冲能量为 0.52 mJ（对应的激光功率密度为 $1.33×10^{15}$ W/cm^2）时，碳炔的产率最高。本研究结果可为碳炔的大规模制备提供重要参考。

2　实　　验

2.1　材　　料

甲醇（CH_3OH，纯度为 98%）购于国药集团化学试剂有限公司，单壁碳纳米管（直径 D:0.8～1.2 nm；铁催化剂质量分数：<35%）购于南京先锋纳米材料科技有限公司。所有化学试剂均为分析级试剂，未经进一步提纯，直接使用。

2.2　碳炔的制备

如图 1 所示，激光烧蚀系统由飞秒激光器、偏振片（型号为 Thorlabs PBSW-808）、光圈、反射镜和聚焦透镜组成。飞秒激光器采用的是波长为 800 nm、最大功率为 8 W、脉宽为 120 fs、重复频率为 1 kHz 的钛蓝宝石激光器。偏振片可以调节激光束的偏振状态。可调光圈用来将激光脉冲能量控制在 0.04～1.48 mJ/pluse 范围内。样品溶液高度约为 6 cm，激光束被反射镜折射后通过焦距为 10 cm 的聚焦透镜，透镜将激光聚焦在样品瓶的底部。因为单壁碳纳米管（SWCNTs）是固体，在甲醇溶剂中易下沉，激光聚焦于样品瓶的底部可以最大程度地烧蚀单壁碳纳米管。用磁力搅拌器搅拌烧杯中的单壁碳纳米管，以保证均匀加工，并在烧杯外部用冷水降温。

为了合成碳炔，将 7 mL 纯度为 98% 的甲醇滴入烧杯中，此甲醇与高效液相色谱仪中使用的流动相相同；然后加入 7 mg 单壁碳纳米管，与烧杯中的甲醇均匀混合。在激光烧蚀期间，为保证液体的均匀性，使用磁力搅拌器不停地搅拌，设置磁力搅拌器的温度为室温，转速为 200 r/min。首先，在相同的烧蚀时间（1.5 h）内，改变激光单脉冲能量（分别为 0.04、0.20、0.36、0.52、0.84、1.16、1.48 mJ）烧蚀样品溶液；然后，在相同的单脉冲能量（0.52 mJ）下，改变烧蚀时间（1、1.5、2、3、4 h）。最后，用孔径为 0.2 μm 的过滤器过滤加工好的样品，以去除固体杂质。
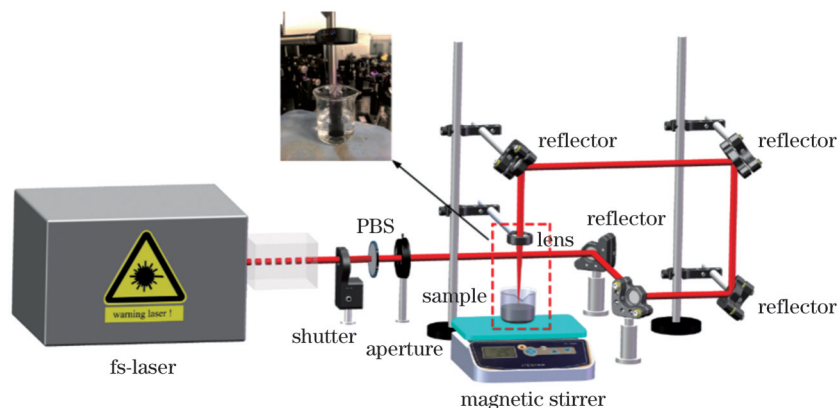

图 1　飞秒激光烧蚀系统示意图

Fig. 1　Schematic illustration of the femtosecond laser ablation system

将样品溶液与银胶体混合（体积比为 1:5），然后将混合物旋涂在衬底上，使用表面增强拉曼光谱仪（SERS）进行拉曼光谱测量[28]。在对碳炔进行表面增强拉曼光谱分析时，用银胶体作为增强剂[29]。采用 532 nm 激光器，光功率为 1 mW，采集时间为 1 s。考虑到测量的均匀性，每个样品随机测量 20 次，测量结果显示出了良好的再现性。

使用双光束紫外光度计（型号为 Shimadzu UV-3600）测量样品溶液的紫外可见吸收光谱，在紫外区域可以检测到碳炔的特征峰。测量波长范围为 200～400 nm，分辨率为 0.1 nm。扫描速度中等，采样间隔为 0.2 nm。从相应的吸收峰中可以推断出碳炔的产率。

使用高效液相色谱仪（型号为岛津 LC-6AD）对样品进行色谱表征。取 5 mL 样品溶液放入色谱分离系统的注射器中。色谱仪使用纯甲醇作为流动相。单次注射 1 mL 时，流速为 5 mL/min。

3　结果与讨论

3.1　性能表征

由于 sp-碳链倾向于通过交联反应重组为更稳定

的碳同素异形体(如 sp^2-碳链或无定形碳),因此碳炔的稳定性较差[30]。sp-碳链对应的表面增强拉曼光谱的特征峰分布在 1800~2200 cm^{-1} 范围内,sp^2-碳链对应的表面增强拉曼光谱分布在 1000~1700 cm^{-1} 范围内[19]。为了研究碳炔的生成,聚焦 sp-碳链的光谱范围,激光单脉冲能量在 0.04~1.48 mJ 之间变化,相应

的拉曼光谱分别展示在图 2 中。由图 2 可以清楚地看到:随着激光单脉冲能量从 0.04 mJ 增大到 0.52 mJ,特征峰的强度逐渐增强;随着激光单脉冲能量从 0.52 mJ 增大到 1.48 mJ,特征峰的强度逐渐减弱;当激光单脉冲能量为 0.52 mJ 时,可以获得最高的强度,这对应于碳炔的最高产率。
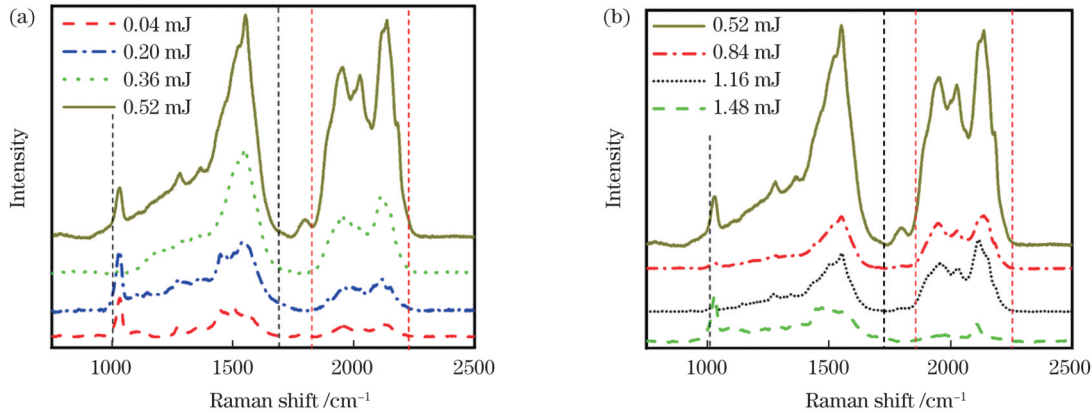

图 2 不同激光单脉冲能量烧蚀的样品溶液的表面增强拉曼光谱。(a) 0.04~0.52 mJ;(b) 0.52~1.48 mJ

Fig. 2 Surface-enhanced Raman spectra of the sample solution ablated with different single-pulse energies. (a) 0.04–0.52 mJ; (b) 0.52–1.48 mJ

由于碳炔短链和长链的特征峰之间存在相当大的重叠,因此可以通过紫外吸收光谱进行进一步验证。测量的吸收光谱如图 3 所示。C_8H_2、$C_{10}H_2$、$C_{12}H_2$、$C_{14}H_2$ 和 $C_{16}H_2$ 对应的吸收峰分别为 225、250、275、298、326 nm[31],C_8H_2 分子的特征峰最明显。当激光单脉冲能量为 0.52 mJ 时,可以获得最强的峰值,这与表面增强拉曼光谱分析结果一致。激光单脉冲能量过低或过高都会降低碳炔的产率。
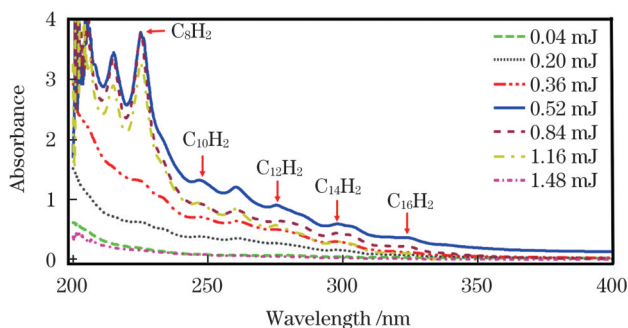

图 3 不同激光单脉冲能量烧蚀样品溶液的紫外吸收光谱

Fig. 3 Ultraviolet absorption spectra of the sample solution ablated with different single-pulse energies

为了探索最佳的激光烧蚀时间,将样品溶液在 0.52 mJ 激光单脉冲能量下分别处理 1、1.5、2、3、4 h,相应的拉曼光谱如图 4(a)所示。sp-碳链是碳的一维同素异形体,具有 sp-碳链的一维线性结构有两种材料,一种是碳碳单键与三键交替连接的碳炔,另一种是碳碳双键连接的聚炔。目前还没有文献报道过聚炔的合成,聚炔尚存在于理论研究阶段,只有个别材料计算类论文提及过聚炔[32]。笔者对样品进行了表面增强拉

曼光谱和紫外可见吸收光谱检测,但仅检测到了 C_8H_2、$C_{10}H_2$、$C_{12}H_2$、$C_{14}H_2$ 和 $C_{16}H_2$ 这几种碳炔的生成,因此 sp-碳链光谱范围内的峰面积代表碳炔的产率。sp-碳链的表面增强拉曼光谱主要位于 1800~2200 cm^{-1} 范围内,sp^2-碳链的表面增强拉曼光谱分布在 1000~1700 cm^{-1} 范围内[19]。笔者分别计算了 sp 和 sp^2 相应峰的面积,计算时不同单脉冲处理时间的样品的基线不同,在图 4(a)中标出了单脉冲处理 3 h 和 4 h 样品的基线,单脉冲处理 1、1.5、2 h 样品的基线位于各曲线的最低点且平行于横轴,利用软件的卷积功能即可直接得出面积值。如图 4(b)所示,飞秒激光烧蚀时间为 1.5 h 时,sp-碳链峰面积最大,这表明最佳处理时间约为 1.5 h。

原始单壁碳纳米管的拉曼光谱如图 4(c)所示,没有经过激光加工的单壁碳纳米管是碳的二维结构,会出现 sp^2 特征峰;而经激光烧蚀 1 h 后的单壁碳纳米管的 sp^2 特征峰略有降低,如图 4(a)所示,这是由于制备好的样品溶液是黑色浑浊的液体,在检测表面增强拉曼光谱前会进行过滤处理。选用滤嘴尺寸为 2 μm 的过滤器过滤掉杂质,此处的杂质主要是飞秒激光烧蚀单壁碳纳米管固体产生的碳管碎片,因此单壁碳纳米管的 sp^2 特征峰略有降低。

采用高效液相色谱仪(HPLC)分离 0.52 mJ 激光单脉冲能量烧蚀的样品溶液,得到了三维色谱图,如图 5(a)所示。该色谱图显示了不同波长与分离时间下的吸收强度[16]。许多碳杂质存在于短波长范围内,滤除碳杂质后,紫外吸收光谱显示了不同长度的碳炔分子。根据高效液相色谱和实时紫外吸收光谱可判断出碳炔的碳链长度,色谱图在约 16 min 时开始出现。图 5(b)~(d)
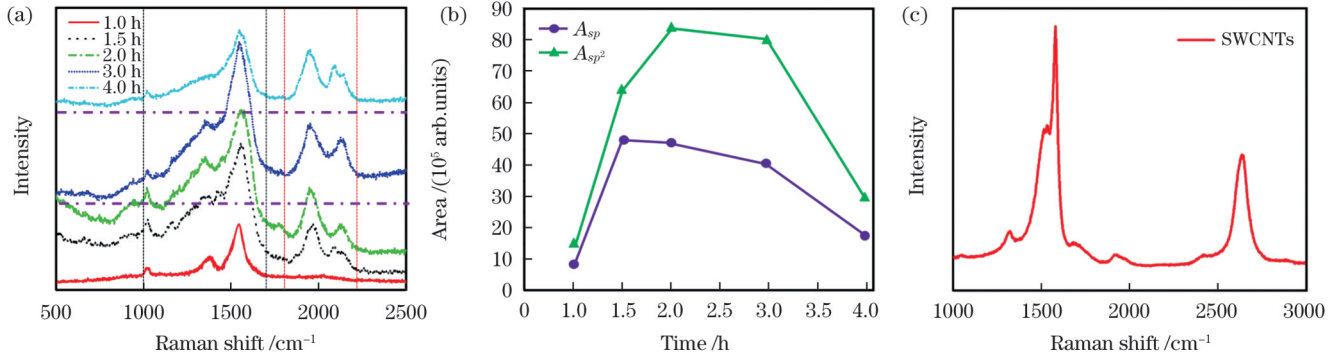
图 4 表面增强拉曼光谱图。(a)样品溶液经 0.52 mJ 激光单脉冲能量烧蚀不同时间后的表面增强拉曼光谱;(b)sp^2-碳链区域(1000~1700 cm^{-1})的积分面积A_{sp^2}、sp-碳链区域(1800~2200 cm^{-1})的积分面积A_{sp}与烧蚀时间的关系;(c)原始单壁碳纳米管的拉曼光谱

Fig. 4 Surface-enhanced Raman spectra. (a) Surface-enhanced Raman spectra of the sample solution ablated with 0.52 mJ single-pulse energy for different time; (b) integrated area (A_{sp^2} and A_{sp}) of sp^2 region (1000–1700 cm^{-1}) and sp region (1800–2200 cm^{-1}) as a function of ablation time; (c) Raman spectra of raw single-walled carbon nanotubes (SWCNTs)
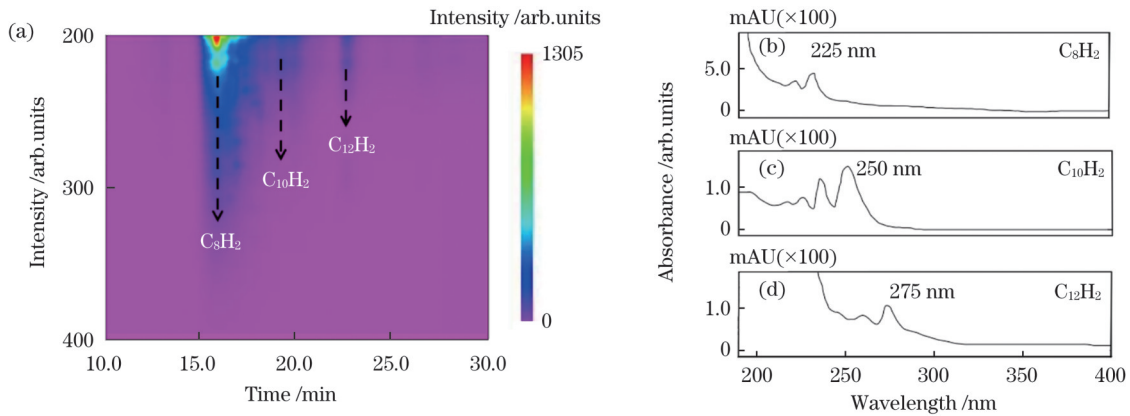

图 5 高效液相色谱图。(a) 0.52 mJ 激光单脉冲能量烧蚀的样品溶液的高效液相三维色谱图;(b)~(d)通过高效液相色谱仪分离获得的碳炔(C_8H_2、$C_{10}H_2$、$C_{12}H_2$)的紫外吸收光谱

Fig. 5 Three-dimensional high-performance liquid chromatography. (a) Three-dimensional high-performance liquid chromatography of the sample solution ablated with 0.52 mJ single-pulse energy; (b)–(d) ultraviolet absorption spectra of polyynes (C_8H_2, $C_{10}H_2$, and $C_{12}H_2$) obtained by high-performance liquid chromatography

显示了相应的紫外吸收谱。225 nm 波长处的吸收峰是 C_8H_2。分离时间约为 19 min 时,在 250 nm 处检测到了 $C_{10}H_2$ 的吸收峰;分离时间约为 23 min 时,在 275 nm 处检测到了 $C_{12}H_2$ 的吸收峰。由于 $C_{16}H_2$ 的浓度较低,在图 5 所示的紫外吸收光谱中未显示出 $C_{16}H_2$。

3.2 烧蚀机理

为了进一步研究烧蚀机理,用 0.52 mJ 激光单脉冲能量烧蚀样品 1.5 h。在烧蚀样品过程中,观察到有气泡产生,如图 6(a)所示。事实上,形成碳炔的碳原子主要来自单壁碳纳米管,还有一少部分来自甲醇[33]。甲醇中碳原子上的化学键(C—H、C—OH)断裂后,一少部分氢原子覆盖碳链末端,碳链停止生长,形成氢封端的碳炔。过量的氢原子相互结合形成氢气,以气泡的形式释放出来。

为了研究激光功率密度对碳炔生成的影响,比较了 $C_{12}H_2$ 长链碳炔的紫外吸收光谱的峰值强度,如图 6(b)所示。由于可调光圈控制着激光单脉冲能量,而样品制备过程中光斑的大小也不同,所以功率密度随激光脉冲

能量非线性变化。表 1 中激光功率密度的计算公式为

$$W = \frac{E}{T \times S},\qquad(1)$$

式中:W 是激光功率密度;E 是激光脉冲能量(0.04~1.48 mJ);T 是脉冲宽度(120 fs);S 是表 1 中的光斑直径对应的光斑面积[34]。

通过调控激光单脉冲能量和光斑面积来保证激光功率密度不变,进行多次实验,最后将所得数据取平均值,得到了 sp 的峰面积,如表 2 所示。可以看出,虽然 sp 的峰面积略有浮动,但都在 47×10^{15} arb. units 附近,说明激光功率密度在 1.33×10^{15} W/cm^2 附近,所获得的碳炔含量较为稳定。笔者又进行了几组激光功率密度超过 1.33×10^{15} W/cm^2 的实验,结果如表 3 所示,可以发现 sp 的峰面积明显减小,这说明激光功率密度饱和阈值(功率密度为 1.33×10^{15} W/cm^2,单脉冲能量为 0.52 mJ,光斑直径为 20 μm,脉宽为 120 fs)还是具有一定的普适性的。
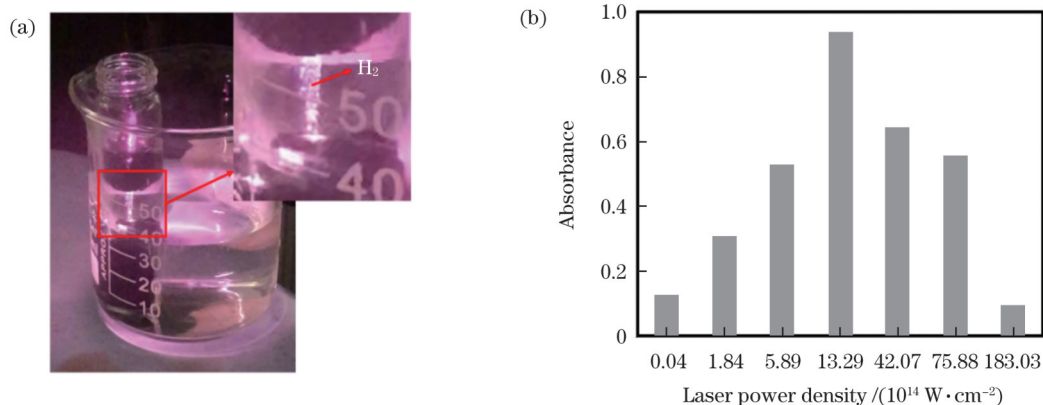
激光功率密度通常需要限于特定值,以避免液体

图 6　紫外吸收光谱的峰值强度。(a)烧蚀过程中产生的氢气气泡;(b)在不同激光功率密度下烧蚀的溶液样品产生的 $C_{12}H_2$ 的紫外吸收光谱的峰值强度

Fig. 6　Peak intensity of ultraviolet absorption spectra. (a) Hydrogen bubble produced during the ablation; (b) peak intensity of ultraviolet absorption spectra of $C_{12}H_2$ from solution sample ablated under different laser power densities

表 1　不同激光脉冲能量和聚焦光斑直径下的功率密度和光通量

Table 1　Power density and fluence obtained under different pulse energies and spot diameters

Pulse energy /mJ	Spot diameter /μm	Power density / (10^{14} W·cm^{-2})	Fluence / (J·cm^{-2})
0.04	102	0.04	0.05
0.20	34	1.84	2.21
0.36	25	5.89	7.33
0.52	20	13.29	16.56
0.84	15	42.07	45.73
1.16	13	75.88	87.44
1.48	9	183.03	231.79

表 2　通过调控激光单脉冲能量和光斑面积保证激光功率密度不变得到的 sp 的峰面积

Table 2　Peak area of sp obtained by adjusting the energy and spot area of single-pulse laser to keep the laser power density constant

Pulse energy /mJ	Spot diameter /μm	Power density / (10^{14} W·cm^{-2})	A_{sp} / (10^{15} arb. units)
0.04	5	13.29	47
0.20	13	13.29	48
0.36	18	13.29	46
0.52	20	13.29	47
0.84	55	13.29	45
1.16	83	13.29	48
1.48	110	13.29	47

表 3　调控激光单脉冲能量和光斑面积保证激光功率密度不变得到的 sp 的峰值面积

Table 3　Peak area of sp obtained by adjusting the energy and spot area of single-pulse laser to keep the laser power density constant

Pulse energy /mJ	Spot diameter /μm	Power density / (10^{14} W·cm^{-2})	A_{sp} / (10^{15} arb. units)
0.04	0.7	13.5	23
0.20	10	13.5	22
0.36	13	13.5	21
0.52	15	13.5	23
0.84	45	13.5	20
1.16	78	13.5	20
1.48	93	13.5	21

$Y_{0.36\,mJ} > Y_{0.20\,mJ} > Y_{0.04\,mJ} > Y_{1.48\,mJ}$。$C_2$ 自由基是碳炔形成的基础,C_2 自由基的形成过程可以表示为 SWCNTs＋ $n\,h\nu \to m\,C_2$[33]。随着激光功率增大,更多的单壁碳纳米管发生解离,碳炔产率逐渐提高;当达到饱和阈值后,继续增大激光功率,将促进 C_2 自由基的碎裂程度,但不会明显改变单壁碳纳米管的解离数量[36],碳炔产率逐渐降低。因此,激光功率密度的饱和阈值对碳炔的合成特别关键,超过这个饱和阈值,碳炔的产率反而会降低。

如图 7 所示,飞秒激光光子的能量高、脉宽小、单色性好,可以精准作用在单壁碳纳米管表面,打破其内部的化学键,使单壁碳纳米管解离成碳片段或 C_2 自由基。C_2 自由基存在一个反向的"第四键",它的强度足以使其被认为是一个化学键,它在碳炔的生长中起着至关重要的作用。

接下来进一步探索飞秒激光影响 C_2 自由基的可能机制。如图 8(a)所示,C_2 基团内部由一个"σ键"和两个"π键"连接,还有两个电子保留在外("反向"第四键),这两个电子指向杂化轨道方向。在没有形成碳炔的情况下,这种向外指向的杂交体仍然保持着高度显

内部发生光学击穿或其他非线性效应[19]。图 6(b)表明最高峰值强度在 $1.33×10^{15}$ W/cm^2(0.52 mJ 激光单脉冲能量)的功率密度下实现,该值可被视为饱和阈值。此时,激光束聚焦在样品瓶底部,到达目标材料的光通量为 16.56 J/cm^2(0.52 mJ 激光单脉冲能量)。根据碳炔在溶剂中吸收峰的位置和吸光度,利用朗伯-比尔定律可以估算溶剂中 $C_{12}H_2$ 的产率[35]。在不同的激光功率密度下,$C_{12}H_2$ 的产率(Y)为 $Y_{0.52\,mJ} > Y_{0.84\,mJ} > Y_{1.16\,mJ} >$

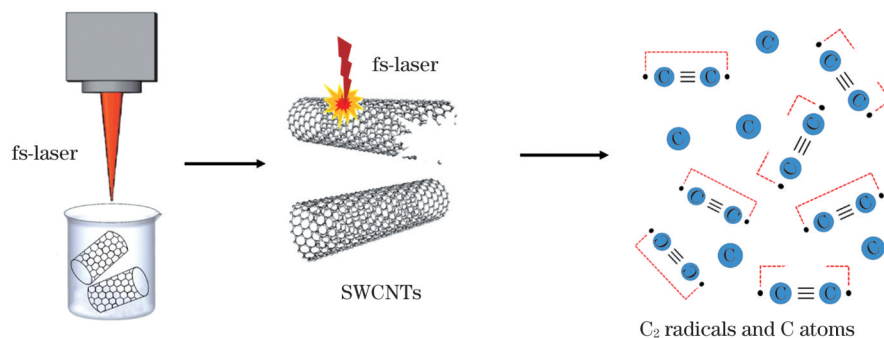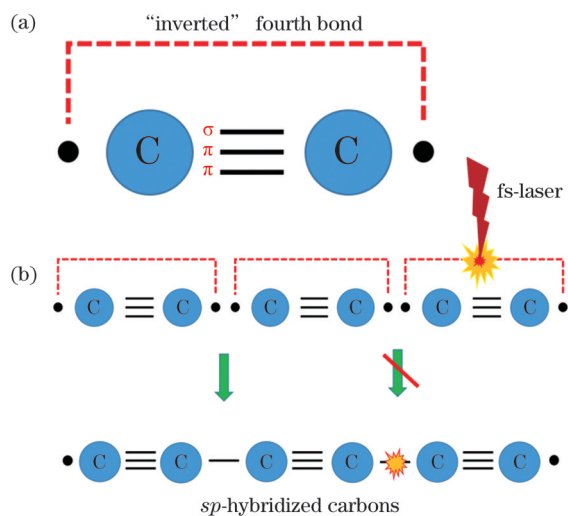图 7 飞秒激光打破单壁碳纳米管化学键生成碳原子或 C_2 自由基的过程

Fig. 7 Femtosecond laser breaking chemical bonds of SWCNTs to form carbon atoms or C_2 free radicals

图 8 形成碳炔的示意图。(a) C_2 自由基的化学键;(b) C_2 自由基的第四键被饱和飞秒激光破坏不能形成 sp-轨道杂交

Fig. 8 Schematic illustration of polyynes forming. (a) Chemical bond of C_2 free radical; (b) the fourth bond of C_2 radical is destroyed by saturated femtosecond laser and can not form sp-orbital hybridization

著的键相互作用[37]。"反向"第四键的能量约为 12~17 kcal/mol[38]。如图 8(b)所示,重复频率为 1 kHz 的飞秒激光可以形成连续的强电离区,激光脉冲功率密度超过了饱和阈值并影响 C_2 自由基之间的连接。进一步增大激光功率将增大 C_2 自由基的碎裂程度,但不会明显改变电离分子的数量;C_2 自由基被破坏后,不能形成 sp-轨道杂交。因此,随着激光功率增大,碳炔的产率先增加后降低。此外,随着烧蚀时间延长,键也会被破坏,从而降低了碳炔的产率。更准确的解释需要精确计算 C_2 簇的结合能。这里给出的激光功率密度饱和阈值和烧蚀时间也可能需要更进一步优化,但它仍然对碳材料的其他激光烧蚀处理具有重要参考价值。

4 结 论

采用飞秒激光烧蚀悬浮在甲醇溶液中的单壁碳纳米管来生成碳炔。对样品溶液进行表面增强拉曼光谱、紫外可见吸收光谱表征,同时利用高效液相色谱仪对碳炔样品溶液进行分离。可以确认制备出了 C_8H_2、$C_{10}H_2$、$C_{12}H_2$、$C_{14}H_2$ 和 $C_{16}H_2$ 碳炔。实验结果表明,当激光单脉冲能量为 0.52 mJ、加工时间为 1.5 h 时可以获得最高的碳炔产率。激光功率密度存在饱和阈值,该饱和阈值与 C_2 自由基的碎裂程度有关,C_2 自由基的"反向"第四键的能量约为 12~17 kcal/mol。激光功率密度超过饱和阈值后会打破 C_2 自由的"反向"第四键,进而影响 C_2 自由基合成碳炔。0.52 mJ 激光单脉冲能量对应的激光功率密度为 1.33×10^{15} W/cm²,此时碳炔的产率最高。本文提出的碳炔的最佳激光烧蚀条件有利于碳炔基薄膜的制备,同时也有利于其他相关实际应用。

参 考 文 献

[1] Xie L Q, Yan L M, Sun C, et al. Force field model and molecular dynamics simulation of polyynes[J]. Computational and Theoretical Chemistry, 2012, 997: 14-18.

[2] Januszewski J A, Tykwinski R R. Synthesis and properties of long [n] cumulenes (n ⩾ 5)[J]. Chemical Society Reviews, 2014, 43(9): 3184-3203.

[3] Casari C S, Tommasini M, Tykwinski R R, et al. Carbon-atom wires: 1-D systems with tunable properties[J]. Nanoscale, 2016, 8 (8): 4414-4435.

[4] Movsisyan L D, Franz M, Hampel F, et al. Polyyne rotaxanes: stabilization by encapsulation[J]. Journal of the American Chemical Society, 2016, 138(4): 1366-1376.

[5] Baughman R H. Dangerously seeking linear carbon[J]. Science, 2006, 312(5776): 1009-1110.

[6] Wakabayashi T, Murakami T, Nagayama H, et al. Raman spectral features of longer polyynes $HC_{2n}H$ (n=4-8) in SWNTs[J]. The European Physical Journal D, 2009, 52(1): 79-82.

[7] Itzhaki L, Altus E, Basch H, et al. Harder than diamond: determining the cross-sectional area and Young's modulus of molecular rods[J]. Angewandte Chemie, 2005, 117(45): 7598-7601.

[8] Nishide D, Wakabayashi T, Sugai T, et al. Raman spectroscopy of size-selected linear polyyne molecules $C_{2n}H_2$ (n=4-6) encapsulated in single-wall carbon nanotubes[J]. The Journal of Physical Chemistry C, 2007, 111(13): 5178-5183.

[9] Malard L M, Nishide D, Dias L G, et al. Resonance Raman study of polyynes encapsulated in single-wall carbon nanotubes[J]. Physical Review B, 2007, 76(23): 233412.

[10] Hu A, Lu Q B, Duley W W, et al. Spectroscopic characterization of carbon chains in nanostructured tetrahedral carbon films synthesized by femtosecond pulsed laser deposition[J]. The Journal of Chemical Physics, 2007, 126(15): 154705.

[11] Chalifoux W A, Tykwinski R R. Synthesis of polyynes to model the sp-carbon allotrope carbyne[J]. Nature Chemistry, 2010, 2(11): 967-971.

[12] Eastmond R, Johnson T R, Walton D R M. Silylation as a protective method for terminal alkynes in oxidative couplings: a general synthesis of the parent polyynes $H(C≡C)_nH$ ($n=4-10, 12$) [J]. Tetrahedron, 1972, 28(17): 4601-4616.

[13] Kang C S, Fujisawa K, Ko Y I, et al. Linear carbon chains inside multi-walled carbon nanotubes: growth mechanism, thermal stability and electrical properties[J]. Carbon, 2016, 107: 217-224.

[14] Cataldo F. Polyynes formation from electric arc in liquid argon in presence of methane[J]. Fullerenes, Nanotubes and Carbon Nanostructures, 2007, 15(4): 291-301.

[15] Zhang Y F, Zhao J W, Fang Y H, et al. Preparation of long linear carbon chain inside multi-walled carbon nanotubes by cooling enhanced hydrogen arc discharge method[J]. Nanoscale, 2018, 10 (37): 17824-17833.

[16] Taguchi Y, Endo H, Kodama T, et al. Polyyne formation by ns and fs laser induced breakdown in hydrocarbon gas flow[J]. Carbon, 2017, 115: 169-174.

[17] Ramadhan A, Wesolowski M, Wakabayashi T, et al. Synthesis of hydrogen-and methyl-capped long-chain polyynes by intense ultrashort laser pulse irradiation of toluene[J]. Carbon, 2017, 118: 680-685.

[18] Tsuji M, Kuboyama S, Matsuzaki T, et al. Formation of hydrogen-capped polyynes by laser ablation of C_{60} particles suspended in solution[J]. Carbon, 2003, 41(11): 2141-2148.

[19] 刘祁文, 刘国东, 李子航, 等. 纳秒激光制备镁合金超疏水表面及其性能研究[J]. 激光与光电子学进展, 2022, 59(5): 0514004. Liu Q W, Liu G D, Li Z H, et al. Preparation and properties of superhydrophobic surface of magnesium alloy by nanosecond laser [J]. Laser & Optoelectronics Progress, 2022, 59(5): 0514004.

[20] 赵强, 万辉, 于圣韬, 等. 飞秒激光制备柔性纳米多孔 Ag 材料的研究[J]. 中国激光, 2021, 48(8): 0802009. Zhao Q, Wan H, Yu S T, et al. Investigation of flexible nanoporous silver materials fabricated by femtosecond laser[J]. Chinese Journal of Lasers, 2021, 48(8): 0802009.

[21] 田梦瑶, 左佩, 梁密生, 等. 飞秒激光加工低维纳米材料及应用[J]. 中国激光, 2021, 48(2): 0202004. Tian M Y, Zuo P, Liang M S, et al. Femtosecond laser processing of low-dimensional nanomaterials and its application[J]. Chinese Journal of Lasers, 2021, 48(2): 0202004.

[22] Zhang K, Zhang Y F, Shi L. A review of linear carbon chains[J]. Chinese Chemical Letters, 2020, 31(7): 1746-1756.

[23] Marabotti P, Peggiani S, Facibeni A, et al. *In situ* surface-enhanced Raman spectroscopy to investigate polyyne formation during pulsed laser ablation in liquid[J]. Carbon, 2022, 189: 219-229.

[24] Zhao J W, Zhang Y F, Fang Y H, et al. Synthesis of polyynes by intense femtosecond laser irradiation of SWCNTs suspended in methanol[J]. Chemical Physics Letters, 2017, 682: 96-100.

[25] Chang W W, Liu F, Liu Y F, et al. Smallest carbon nanowires made easy: long linear carbon chains confined inside single-walled carbon nanotubes[J]. Carbon, 2021, 183: 571-577.

[26] Zaidi A A, Hu A, Henneke D E, et al. Femtosecond laser irradiation of liquid alkanes: mechanism of polyyne formation[J]. Chemical Physics Letters, 2019, 723: 151-154.

[27] Tsuji M, Tsuji T, Kuboyama S, et al. Formation of hydrogen-capped polyynes by laser ablation of graphite particles suspended in solution[J]. Chemical Physics Letters, 2002, 355(1/2): 101-108.

[28] Liu Y, Feng J J, Li Z Y, et al. Double-groove terahertz chirped grating waveguide tube for gas pressure detection[J]. Laser Physics Letters, 2019, 16(5): 056202.

[29] Lee P C, Meisel D. Adsorption and surface-enhanced Raman of dyes on silver and gold sols[J]. The Journal of Physical Chemistry, 1982, 86(17): 3391-3395.

[30] Zhang A, Feng J J, Yan J C, et al. Laser reshaping of gold nanoparticles for highly sensitive SERS detection of ciprofloxacin [J]. Applied Surface Science, 2022, 583: 152543.

[31] Shi L, Rohringer P, Suenaga K, et al. Confined linear carbon chains as a route to bulk carbyne[J]. Nature Materials, 2016, 15 (6): 634-639.

[32] Abdurahman A, Shukla A, Seifert G. *Ab initio* many-body calculations of static dipole polarizabilities of linear carbon chains and chainlike boron clusters[J]. Physical Review B, 2002, 66(15): 155423.

[33] Pan B T, Xiao J, Li J L, et al. Carbyne with finite length: the one-dimensional *sp* carbon[J]. Science Advances, 2015, 1(9): e1500857.

[34] Poveda J C, Guerrero A, Álvarez I, et al. Multiphoton ionization and dissociation of naphthalene at 266, 355, and 532 nm[J]. Journal of Photochemistry and Photobiology A: Chemistry, 2010, 215(2/3): 140-146.

[35] Cataldo F, Ursini O, Angelini G. Kinetics of polyynes formation with the submerged carbon arc[J]. Journal of Electroanalytical Chemistry, 2007, 602(1): 82-90.

[36] Lubman D M, Naaman R, Zare R N. Multiphoton ionization of azulene and naphthalene[J]. The Journal of Chemical Physics, 1980, 72(5): 3034-3040.

[37] Wu W, Gu J J, Song J S, et al. The inverted bond in [1.1.1] propellane is a charge-shift bond[J]. Angewandte Chemie International Edition, 2009, 48(8): 1407-1410.

[38] Shaik S, Danovich D, Wu W, et al. Quadruple bonding in C_2 and analogous eight-valence electron species[J]. Nature Chemistry, 2012, 4(3): 195-200.

Preparation of Polyynes Based on Femtosecond Laser Ablation of Single-Walled Carbon Nanotubes

Chen Wenbin[1], Feng Jijun[1*], Liao Yang[2], Xia Xincheng[1], Jiang Wei[1], Ren Wenbo[1], Luo Tao[3], Zhao Xinluo[3**]

[1]*Shanghai Key Laboratory of Modern Optical System, School of Optical-Electrical and Computer Engineering, University of Shanghai for Science and Technology, Shanghai 200093, China*;

[2]*State Key Laboratory of High Field Laser Physics, Shanghai Institute of Optics and Fine Mechanics, Chinese Academy of Sciences, Shanghai 201800, China*;

[3]*Department of Physics, Institute of Low-Dimensional Carbons and Device Physics, Shanghai University, Shanghai 200444, China*

Abstract

Objective Research on carbon nanotubes (CNTs) and graphene is very mature, and has led to substantive breakthroughs in

electronics; however, some problems remain. For example, the experimental process for obtaining high-purity, semiconducting CNTs is complex, and the ability to adjust the bandgap of graphene is restricted. However, both these materials encounter limitations when used in electronic devices, among which, Young's modulus and stiffness are the key criteria. Theoretical research has shown that polyynes exhibit better Young's modulus and stiffness than graphene, CNTs, and diamond. In particular, polyynes have very high tensile strength, and their performance is unaffected by bending deformation, which cannot be achieved using CNTs and graphene. Thus, the limitations of single-walled CNTs (SWCNTs) and graphene can be overcome. Moreover, polyynes demonstrate excellent electrical properties (such as π-electronic system) and good hardness (i.e., 40 times that of diamond), providing potential applications in aerospace and nanotechnology. However, polyynes suffer from instability, high preparation costs, and low concentrations. In this study, based on femtosecond laser ablation technology, polyynes were prepared using a Ti：sapphire femtosecond laser with the repetition rate of 1 kHz to ablate SWCNTs suspended in methanol. The optimal laser power and processing time for preparing polyynes were explored, and the mechanism of polyyne synthesis was detailed, which will play an important role in the large-scale preparation of polyynes.

Methods   Various methods have been adopted to synthesize polyynes, which can be roughly divided into electrochemical (e.g., oxidation couples and electric arcs) and laser ablation (e.g., gas and liquid phases) techniques. Oxidation coupling is complex and impurities can be easily introduced. Arc discharge is commonly used to generate carbon chains, with the arc discharge in water. However, it cannot control the groups capped at both ends, which limits the stability and electronic properties of polyynes. For laser ablation, gas-phase facilities are complex, and typically require high airtightness and temperature control. Nevertheless, owing to its comparatively low cost, variety of target materials, and ablation surroundings, liquid-phase laser ablation has been widely employed to prepare carbon nanostructures at room temperature. Nanosecond and femtosecond lasers are the most commonly used to achieve this. However, nanosecond lasers have a significant thermal effect, which is not conducive to the formation of polyynes at room temperature. In contrast, femtosecond lasers have little thermal effect and high photon energy, which is beneficial for breaking the chemical bonds of SWCNTs for polyyne preparation. Accordingly, liquid-phase laser ablation with a femtosecond laser was selected for this study.

Results and Discussions   In this work, for SERS characterization, the sample solution was mixed with a silver colloid at the volume ratio of 1∶5 and then spin-coated onto a silicon substrate for Raman spectrum measurement. The characteristic peak intensity of single-pulse laser energy increases with the increasing laser energy from 0.04 to 0.52 mJ, and decreases with the increasing laser energy from 0.52 to 1.48 mJ. When the single-pulse laser energy is 0.52 mJ, the highest intensity is obtained with the highest yield of polyynes. Because there is considerable overlap between the characteristic peaks of the short and long polyyne chains, further validation could be realized using the UV absorption spectrum. The corresponding absorption peaks of C_8H_2, $C_{10}H_2$, $C_{12}H_2$, $C_{14}H_2$, and $C_{16}H_2$ are approximately 225, 250, 275, 298, and 326 nm, respectively. Thus, long-chain polyynes containing more than 12 carbon atoms are generated. The characteristic peak of the C_8H_2 molecule was the most evident. In particular, the strongest peaks are realized for the ablation case with the pulse energy of 0.52 mJ, which is consistent with the SERS analysis. A pulse energy that is too low or too high deteriorates the generation of polyynes. Therefore, 0.52 mJ can be determined as the best single-pulse laser energy for preparing polyynes. The corresponding peak areas for sp and sp^2 are further calculated. The peak area of sp carbon chain in the spectral range represents the polyyne concentration. The sp carbon peak area is the largest with the femtosecond laser ablation time of 1.5 h. This indicates that the optimal processing time is approximately 1.5 h. For the femtosecond laser with the repetition rate of 1 kHz, a continuous strong ionization region can be formed, where the laser pulse energy exceeds the saturation threshold (1.33×10^{15} W/cm^2) and affects the connections between C_2 radicals. Further increasing the laser power enhances the extent of fragmentation, but does not appreciably change the number of ionized molecules. Subsequently, the C_2 radical is destroyed and cannot form sp orbital hybridization. Thus, the polyyne yield initially increases and then decreases. Moreover, with an increase in the ablation time, the bond would also be destroyed, and thus, the yield would decrease.

Conclusions   Laser ablation of SWCNTs suspended in methanol was performed using a Ti∶sapphire femtosecond laser. From characterization via Raman spectroscopy, high-performance liquid chromatography, and ultraviolet absorption spectroscopy, linear hydrogen-capped polyynes (C_nH_2: n＝6, 8, 10, 12, 14, and 16) were confirmed, and the main product was C_8H_2.

The highest yield of polyynes was realized at 1.5 h ablation with the laser power density of 1.33×10^{15} W/cm^2. This saturation threshold may correspond to the extent of C_2 radical fragmentation. The presented optimal laser ablation conditions for polyynes will facilitate the preparation of polyyne-based films and favor other practical applications.

Kay words   laser technique; polyynes; femtosecond laser ablation; laser power density saturation threshold; single-walled carbon nanotubes